Korean J. Chem. Eng., **27**(3), 983-990 (2010)
DOI: 10.1007/s11814-010-0130-x

Mesoporous silica synthesis in sub- and supercritical carbon dioxide

Byung-Soo Chun*, Phillip Pendleton,†, Alexander Badalyan**, and Sun-Young Park****

*Division of Food Science and Biotechnology, Pukyong National University, Busan, Korea
**Center for Molecular and Materials Sciences, Sansom Institute,
School of Pharmacy and Medical Sciences, University of South Australia, Adelaide, SA 5000, Australia
(*Received 27 May 2009 • accepted 23 August 2009*)

Abstract−Mesoporous silicas were synthesized from sodium silicate ($Na_2Si_3O_7$) and tetraethylorthosilicate (TEOS) with Pluronic F127 (polyethylene oxide-polypropylene oxide-polyethylene oxide, $EO_{106}PO_{70}EO_{106}$) triblock copolymer using sub- and supercritical carbon dioxide ($SubCO_2$ and SCO_2) respectively, as solvents. Templates were removed using liquid carbon dioxide (LCO_2) and SCO_2. The most efficient template removal was achieved by LCO_2 - 92.7% (w/w), followed by LCO_2 with ethanol entrainer - 85.6% (w/w), and by methanol - 78.8% (w/w). The best efficiency of template removal by SCO_2 was 50.7%. Values of specific surface areas, A_{BET}, were increased by 10% with the increase of an ageing time from 6 to 24 hours for $Na_2Si_3O_7$-based silicas at aqueous synthesis conditions, whereas the use of SCO_2 reduced this value by 19.4%. For TEOS-based silicas synthesized using SCO_2, A_{BET} values increased by 3.8 times. Application of SCO_2 for synthesis of TEOS-based silicas resulted in higher mesopore volumes of 0.719 and 1.241 mL/g with an average mesopore width varying from 3.4 to 3.9 nm. Although $Na_2Si_3O_7$-based silicas have almost similar mesopore width range, their mesopore volumes were 7 times less than those for TEOS-based silicas. Formation of mesopores in $Na_2Si_3O_7$- and TEOS-based silicas was at the expense of micropores when synthesized in SCO_2.

Key words: Mesoporous Silica Synthesis, Mesopore Development, Pluronic F127 Triblock Copolymer, Liquid Carbon Dioxide Solvent, Supercritical Carbon Dioxide Solvent

INTRODUCTION

Mesoporous materials offer themselves as a convenient reservoir for controlled drug delivery systems; the well-defined porosity readily accepts organic guest molecules [1]. Zhao et al. [2] presented several recipes for the synthesis of mesoporous silica structures with pores in the range 2.0-30.0 nm. One of those methods employed tri-block copolymers from the Pluronic® family of ethylene oxide-propylene oxide-ethylene oxide nonionic surfactants (Pluronic® 123 and Pluronic® 127) and various silica precursors: silicon alkoxides such as tetramethylorthosilicate (TMOS) [2,3], TEOS [2,4,5], tetrabutylorthosilicate (TBOS) [6], tetrapropylorthosilicate (TPOS) [2]; and sodium silicates [4,7,8]. Although the formation of mesoporosity from TMOS is faster than from TEOS and TBOS, TEOS is regarded as the most efficient and, therefore, preferred silica precursor [9]. Mesoporous silica synthesis is usually carried out in aqueous media with various pH levels (basic or acidic synthesis), at various temperatures (hydrothermal method) and for various reaction times. Elevated temperatures and longer reaction duration translated to mesopores of wider pore size and thinner wall structure [2,4]. Similar effects were achieved by increasing the copolymer Pluronic® 123 content in a polymer mixture with Pluronic® 127 [10].

Cooper [11] and Hanrahan [12] reported the synthesis of ordered porous polymeric structures with SCO_2, which has been proposed as an alternative solvent to conventional organic solvents in solvent-intensive processes. Both LCO_2 and SCO_2 may be regarded as good inorganic solvents for the synthesis of porous materials because of their modest critical temperature and pressure, high diffusivity, low dynamic viscosity, extremely low surface tension and surface energy, which translates to extraordinary wetting properties [11], and controllable solubility and non-cohesion [13]. The above properties allow to control specific surface area and mesopore size through pore swelling of synthesized materials by variation of SCO_2 conditions (pressure and temperature adjustment) without affecting mesopore order [12]. Such properties, together with non-toxicity, non-flammability, non-reactivity, cheap cost, and simplicity in use, play a key role in the emerging applications of LCO_2 and SCO_2 in various areas, including the production of stable mesoporous materials with a uniform pore sizes [14].

For the removal of polymeric templates, refluxing with liquid organic solvents, such as ethanol [2], ethanol-plus-H_2SO_4, ethanol-plus-NaOH and ethanol-plus-HCl mixtures [15] has been demonstrated. The template removal efficiency was not impressive, reaching 71±3% [5]. Very often, liquid organic solvent template extraction was followed by high temperature (823-850 K) calcination in an air atmosphere [2,10]. Among these template extraction methods, calcination is referred to as 100% effective due to the total thermal decomposition of organic copolymer template. Grieken et al. [5] employed SCO_2 with and without organic liquid co-solvent resulting in up to 81% of template removal. Kawi and Lai [16] reported the inability of SCO_2 alone to remove organic template, whereas the addition of methanol or water as co-solvent increased template removal efficiency by 86.3 and 93.6%, respectively. Although the application of SCO_2 with or without organic co-solvent modifier cannot reach 100% organic template removal, it is regarded as a

†To whom correspondence should be addressed.
E-mail: phillip.pendleton@unisa.edu.au

Table 1. Experimental conditions for mesoporous materials synthesis

Sample	Reaction condition			Silica source	Ageing time, (hour)	Calcination	
	T, K	P, MPa	Time, (hour)			T, K	Time, hour
1-N	293.15	0.1	24	$Na_2Si_3O_7$	6	818.15	7
2-N	293.15	0.1	24	$Na_2Si_3O_7$	24	818.15	7
3-N	338.15	0.1	24	$Na_2Si_3O_7$	6	818.15	7
4-VCO_2	293.15	5.3	24	$Na_2Si_3O_7$	6	818.15	7
5-SCO_2	338.15	13.6	24	$Na_2Si_3O_7$	24	818.15	7
6-N	338.15	0.1	24	TEOS	24	818.15	7
7-SCO_2	338.15	13.6	24	TEOS	24	818.15	7
8-SCO_2	325.15	12.2	12	TEOS	24	818.15	7

preferred solvent due to better solvating power compared to other organic solvents: mild extraction conditions which do not significantly affect the structure of mesoporous silicas, surface hydroxyl groups preservation, and larger mesopore size development when compared with high-temperature calcination [9].

Mesoporous silica synthesis and organic template removal using SCO_2 as alternative solvent has several advantages, such as prevention of pore collapse, superior penetration into pores, control of mesopore diameter by variation of CO_2 properties, and pore surface functional groups preservation due to mild synthesis conditions. Several experimental parameters, such as silica sources, ingredients' molar ratios, and ageing times and temperatures were targeted in a number of studies on mesoporous materials synthesis [5,14]. Each of these variables affects pore size distribution and the extent of localized order within the synthesized material structure. No information exists about the application of sub-critical CO_2 for mesoporous silica synthesis, and LCO_2 for organic template removal. The ability of various liquid organic solvents, LCO_2 and SCO_2 to remove the polymeric template, along with an impact of various silica sources, CO_2 physical properties and various synthesis conditions on the development of silica mesoporosity, was tested in the present research.

EXPERIMENTAL

1. Materials

Two silica sources via $Na_2Si_3O_7$ (ex Sigma) and TEOS (ex Sigma) were chosen; Pluronic F127 as the nonionic tri-block copolymer $EO_{106}PO_{70}EO_{106}$ was used as the porogen.

One synthesis route, hydrothermal, consisted of 1.5 g of Pluronic F127 dissolved by stirring in 90 mL of 2 M HCl for 20 hours at room temperature, followed by cooling to 288.15 K. To produce particles, 4.8 mL of either $Na_2Si_3O_7$ or TEOS was slowly added to the mixture producing molar concentrations as $1SiO_2$: 0.778NaOH : 0.00735Pluronic F127 : 6HCl : $162H_2O$ or 1TEOS : 0.00735Pluronic F127 : 6HCl : $155H_2O$. As variations in the synthesis process, the resultant mixtures were stirred at 293.15 or 333.15 K for 24 hours and aged without stirring at 373.15 K for 6 or 24 hours. The solid precipitates were filtered by using a nylon membrane filter (0.45 μm pore size) and dried at room temperature for 24 hours.

The synthesis procedure under $SubCO_2$ and SCO_2 conditions was carried out as follows: 30 mL of the 2 M HCl solution mixed with copolymer and 2 M HCl were loaded into the reactor, followed by the silica source, which was added while stirring. Then, the internal volume of the reactor was filled by liquid CO_2. First, the desired experimental synthesis temperature was reached, and later an experimental pressure was developed. The mixture in the reactor was observed through the view cell. After a reaction time of 24 hours, the experimental pressure in the reactor was reduced to atmospheric, and the resultant mixture collected. This mixture was subjected to filtration, calcinations and isotherm nitrogen adsorption.

The polymeric templates were removed by one of three different methods. In the first method, 100 mL of organic solvents (methanol, ethanol, acetone, n-hexane, and iso-propanol) was added to beakers, each filled with 0.4 g of the synthesized polymeric material from the same batch and agitated at 298.15 K for 24 hours. A second tem-

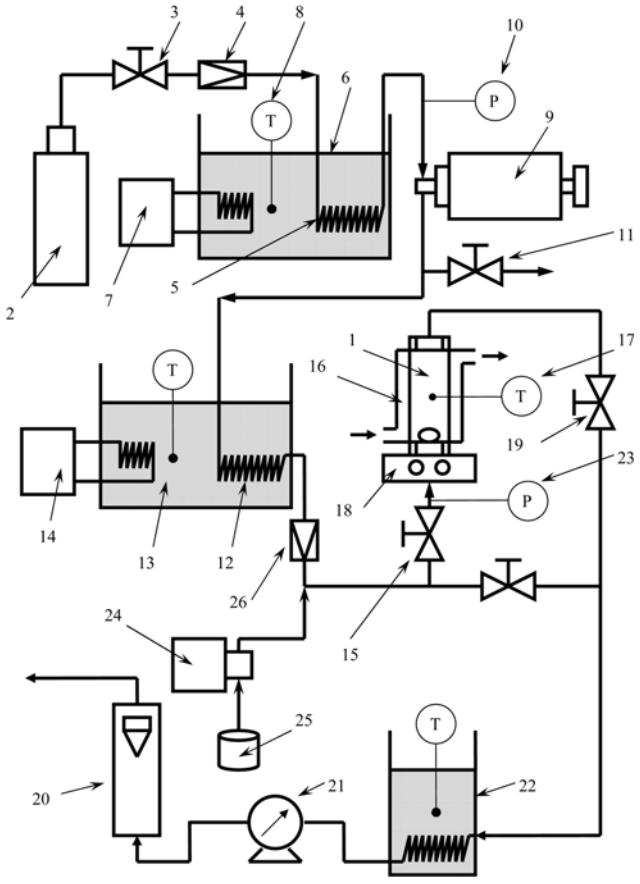

Fig. 1. Experimental apparatus for silica synthesis.

plate removal procedure involved 0.8 g of the silica placed in a high-pressure reactor filled with CO_2 either with or without ethanol as co-solvent at CO_2 sub- and supercritical conditions. The CO_2 flowrate was maintained at 4 mL/min with 3% (vol./vol.) of ethanol entrainer. The reactant mixtures were stirred at 300 rpm for 45 or 90 min at various temperatures and pressures in LCO_2 and SCO_2. The third method involved calcination of synthesized porous materials in an atmospheric furnace at 818.15 K for 7 hours with a summary of experimental conditions given in Table 1.

2. Supercritical CO_2 Apparatus

Fig. 1 shows a schematic of a flow-through-type supercritical fluid apparatus. LCO_2 (Food Grade, BOC Gases, Australia) was delivered to the reactor (1) from high pressure cylinders (2). The reactor with internal volume of 6.0×10^{-5} m^3 (I.D.=22×10^{-3} m) was made of 316 stainless steel, and its internal surface was lined with Teflon. Two sapphire glass windows were used for visually monitoring the synthesis. From the high-pressure cylinder, LCO_2 passed through a pressure regulator (3), filter (4) and coiled tube (5) placed in a pre-cooled bath (6) filled with ethylene glycol/water (50% w/w) solution kept at 253.15 K. These low temperatures were developed by a freezer (7) and measured by a type-K thermocouple (8) with an accuracy of ±0.05 K. The LCO_2 then entered a positive-displacement, controlled-volume, metering pump (Milroyal B, USA) (9). At this temperature, CO_2 remained in a liquid state, thus excluding cavitation in the pump. This piston pump delivered LCO_2 to the reactor at a flowrate constant to within ±1%. The LCO_2 pressure prior to the piston pump was monitored by a Bourdon pressure gage (10). A safety/relief valve (11) was used to control pressure after the piston pump.

After the piston pump, the LCO_2 stream passed through another coiled tube (12) placed in the second bath (13) filled with water and equipped with an electric temperature-controlled system (14). Here, LCO_2 was pre-heated to ±0.5 K of the reactor temperatures before entering the reactor via an ON/OFF manual shut-off valve (15). Such an arrangement eliminated the temperature gradient inside the reactor. To maintain a constant temperature in the reactor, water was circulated in the jacket (16) around the reactor. An ABB Commander temperature controller with Type-K thermocouple (17) was used for the temperature monitoring within ±0.1 K and control within ±0.05 K. A magnetic stirrer (18) provided uniformity of fluid temperature in the reactor.

Pressure in the reactor was controlled by maintaining a constant CO_2 flowrate by a Swagelok metering needle-valve (19) with an accuracy of ±0.005 MPa. CO_2 flowrate measurements were taken by a calibrated rotameter (20). A Parkinson Cowan totalizer gas meter (21) with accuracy of $\pm10^{-4}$ m^3 was used to measure the total volume of CO_2 passed through the reactor. This volume was converted to mass at normal conditions (0.1 MPa and 298.15 K), since CO_2 volume totalizing measurements were made at ambient conditions after the heat-exchanger (22), which brought the temperature of the CO_2 stream leaving the reactor to 298.15 K. Pressure was measured by a high-accuracy absolute pressure transmitter (Cole Parmer) (23) with a digital readout with an accuracy of ±0.15% of full scale (0.1 to 41.4 MPa).

Food-grade ethanol as a co-solvent to CO_2 was added by a dual-plunger HPLC entrainer pump (ICI Instruments) (24) from an ethanol reservoir (25) after a non-return valve (26) to prevent accidental flow of ethanol to CO_2 cylinder.

3. Nitrogen Adsorption Measurements

Porosity development within the materials was assessed by using an automatic manometric gas adsorption apparatus [17]. This apparatus was calibrated with a certified standard specific surface area material (silica-alumina, SRM® 1897, NIST, Gaithersburg, USA) with a reported multipoint A_{BET} value of 258.32±5.29 m^2/g. Each silica sample was pre-heated and evacuated at 473.15 K for 8 hours at a pressure $<1\times10^{-4}$ Pa. Dead-volume measurements were carried at 77 K using ultra high purity grade gaseous helium (99.999%, BOC Gases Australia). To ensure helium removal, the sample was again degassed as above for 2 hours. Nitrogen adsorption was carried out at 77 K in a relative pressure range (relative to atmospheric pressure) from 0 to 1 using ultra high purity grade gaseous nitrogen (99.999%, BOC Gases Australia). A_{BET} area for this standard silica-alumina material was calculated using weight mean-least squares method described earlier [18]. This evaluated A_{BET} value of 254.57±0.78 m^2/g agrees with that reported by NIST within 1.5%, and is within the combined experimental uncertainty of both measurements. Similar sample preparation and nitrogen adsorption procedures were used for characterization of the synthesized samples.

A_{BET} values for these samples were evaluated in the relative pressure range from 0.05 to 0.35 as described earlier [18] (the linear regression coefficient of the BET plot >0.9990). Pore volumes of the above samples were evaluated by using the α_s-plot method [19]. As a standard adsorption isotherm for the generation of α_s-plot we used nitrogen adsorption data on Aerosil 200 at 77 K [20]. A_{BET} for Aerosil 200 is equal to 207.81±1.89 m^2/g. These data were processed by using a weighted mean least squares method for the calculation of pore volumes and their combined standard uncertainties (CSUs) [20]. It is customary to express the total specific pore volume of an adsorbent, V_{pore}^{total}, as the liquid volume adsorbed at certain value of relative pressure, typically p/p_o=0.95 [21]. We thus converted the gaseous nitrogen volume adsorbed at this value of relative pressure into a liquid volume of nitrogen. If the sample does not contain micropores, then this volume is referred to as a mesoporous volume, V_{meso}. For mixed-pores materials, V_{meso} is determined as the difference between the V_{pore}^{total} and micropore volume, V_{micro}.

Pore size distribution is used for the characterization of porous materials. We used the classification for micropore, mesopore and macropore width, w_p, according to the IUPAC recommendations as follows: micropores have width $w_p<2$ nm, mesopores have width $2<w_p<50$ nm, and macropores have width $w_p>50$ nm [22]. Micropore size distribution was analyzed by using the Saito and Foley method for cylindrical pore geometry [23]. For the application of this method to the experimental adsorption data, value for static polarizability, α_S, for amorphous silica was calculated according to the Clausius-Mosotti equation [24] using data for atomic polarizability [25], and the value of diamagnetic susceptibility, χ_S, was adopted from [26]. Mesopore size distribution was evaluated using Barett, Joyner and Halenda (BJH) method [27]. BJH method was applied to data from desorption branches of isotherms.

RESULTS AND DISCUSSION

1. Organic Template Removal

The results for polymeric template removal by various methods

are given in Tables 2 to 4. As a benchmark for efficiency of polymeric template removal we used calcination results as 100% template removal. Among liquid organic solvents, methanol performed more efficiently than others due to its higher solvation power as a more polar solvent by removing almost 78.8% of template (see Table 2). Efficiency of template extraction with ethanol in our experiments is lower by ≈3.2% than that reported by Grieken et al. [5]. It was surprising to observe that template removal by n-hexane was more efficient than by more polar acetone.

We achieved ≈92.7% of template removal efficiency by treatment with liquid LCO_2 at 298 K and 12.3 MPa for 45 min (see Table 3). Although LCO_2 and SCO_2 densities in our experiments were almost similar, varying from 849.02 to 850.22 kg/m^3 [28], the efficiency of template extraction by SCO_2 was lower than by LCO_2 (see Table 3). Solubility of CO_2 in the polymeric template increases with temperature decrease and pressure increase [29]. The effect of pressure increase from 12.3 to 35.8 MPa on the CO_2 solubility is not significant compared to the effect of temperature variation from 298.15 to 338.15 K. Therefore, template removal conditions at 298.15 K and 12.3 MPa resulted in better solubility of LCO_2 in the polymeric template, and, consequently, greater removal of the template. Ethanol addition as co-solvent decreased this solubility even further. Increasing the duration of template removal from 45 to 90 min at supercritical temperature of 308 K and 18.2 MPa increased this efficiency by ≈3 times. Higher temperatures and lower pressures for supercritical conditions were employed by Grieken et al. [5] with the reported template extraction efficiency ≈30% higher than the best efficiency achieved by SCO_2 in our experiments.

As a non-polar solvent, LCO_2 better removes hydrophilic triblock copolymer template than various organic solvents studied in the present research, thus getting better access to micropores in the silica walls [5], although we did not observe the narrowing mesopore size distribution.

2. Silica Characterization via Nitrogen Adsorption/Desorption

Table 5 and Figs. 2-6 show the effect of different synthesis conditions on the adsorption properties of synthesized mesoporous silica

Table 2. Extraction efficiencies of template removal by liquid organic solvents

Parameter	Calcination	Solvent for template removal				
		Methanol	Ethanol	n-Hexane	Iso-propanol	Acetone
M_t, g	0.1077	0.0849	0.0698	0.0552	0.0410	0.0372
Efficiency, %	100.0	78.8	64.8	51.3	38.1	34.5

Table 3. Extraction efficiencies of template removal by CO_2 without ethanol entrainer

P, MPa	12.3	18.2	24.0	30.0	35.8
T, K	298.15	308.15	318.15	328.15	338.15
CO_2 density, kg/m^3 [28]	849.02 (*l*)	849.93 (s)	849.39 (s)	850.22 (s)	849.57 (s)
Time, min	45	90	45	45	45
Mass of removed template, g	0.1996	0.1092	0.0397	0.0566	0.0308
Efficiency, %	92.7	50.7	18.4	26.3	14.3

Note: l-liquid state; s-supercritical state

Table 4. Extraction efficiencies of template removal by CO_2 with ethanol entrainer

P, MPa	12.3	18.2	24.0	30.0	35.8
T, K	298	308	318	328	338
Time, min	45	45	90	45	45
Mass of removed template, g	0.1843	0.0489	0.0202	0.0516	0.0208
Efficiency, %	85.6	22.7	9.4	24.0	9.7

Table 5. Results for gaseous nitrogen adsorption

Sample	Moisture content, %	A_{BET}, m^2/g	V_{micro}, cm^3/g	α_S-range	V_{meso}, cm^3/g	V_{pore}^{total}, cm^3/g	w_{micro} and w_{meso}, nm
1-N	3.76	503.9±1.9	0.212±0.002	0.973-1.418	0.023±0.004	0.235±0.002	0.75 and 3.81
2-N	2.97	556.3±1.1	0.269±0.004	1.024-1.553	0.046±0.005	0.315±0.003	0.81 and 4.27
3-N	2.60	124.9±0.2	0.067±0.001	1.683-2.749	0.034±0.001	0.101±0.001	0.81 and 3.37
4-VCO_2	6.20	480.4±1.9	0.209±0.007	1.009-1.439	0.074±0.008	0.283±0.004	0.70 and 3.34
5-SCO_2	3.80	448.1±1.3	0.150±0.004	0.970-1.518	0.175±0.005	0.325±0.003	0.71 and 3.51
6-N	4.90	218.5±0.8	0.019±0.004	0.618-0.731	0.406±0.005	0.425±0.004	0.96 and 3.44
7-SCO_2	7.59	809.5±3.3	0.175±0.014	1.019-1.484	0.719±0.017	0.894±0.010	0.69 and 3.74
8-SCO_2	13.64	825.5±3.5	0.090±0.004	0.551-0.961	1.241±0.014	1.331±0.013	0.72 and 3.88

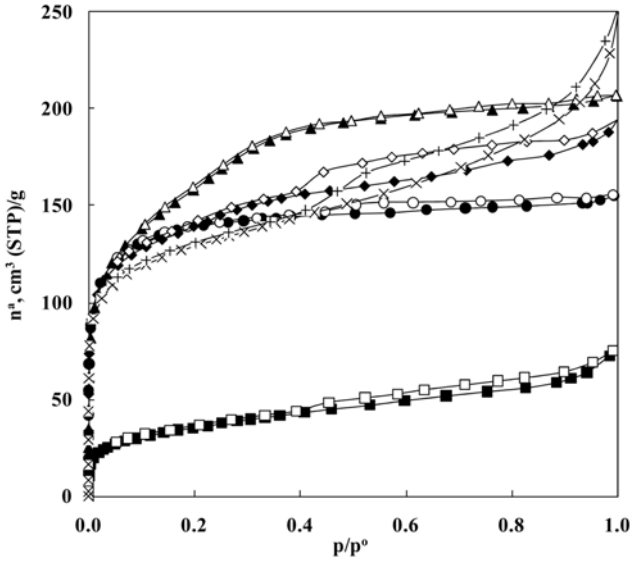

Fig. 2. Nitrogen adsorption/desorption isotherms for samples synthesized from $Na_2Si_3O_7$.
1-N: ● - adsorption, ○ - desorption; 2-N: ▲ - adsorption, △ - desorption; 3-N: ■ - adsorption, □ - desorption; 4-VCO_2: ◆ - adsorption, ◇ - desorption; 5-SCO_2: × - adsorption, + - desorption.

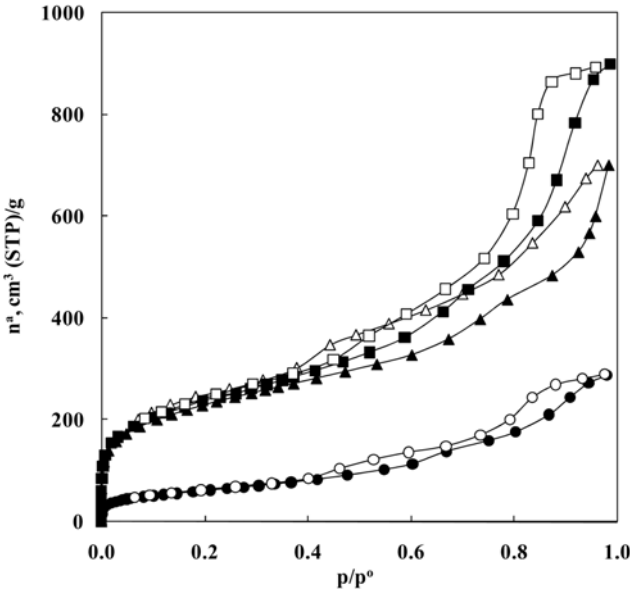

Fig. 3. Nitrogen adsorption/desorption isotherms for samples synthesized from TEOS.
6-N: ● - adsorption; ○ - desorption; 7-SCO_2: ▲ - adsorption; △ - desorption; 8-SCO_2: ■ - adsorption, □ - desorption.

materials obtained by template removal by calcination. Each experimental point on adsorption/desorption branches of nitrogen isotherms is accompanied with its CSU.

As follows from Fig. 2, isotherms for all samples synthesized from $Na_2Si_3O_7$ are of complex (mixed) types: Type I with H4 hysteresis loop according to IUPAC classification [30] or Type Ib according to Rouquerol et al. [21]. Earlier [21], such narrow hysteresis

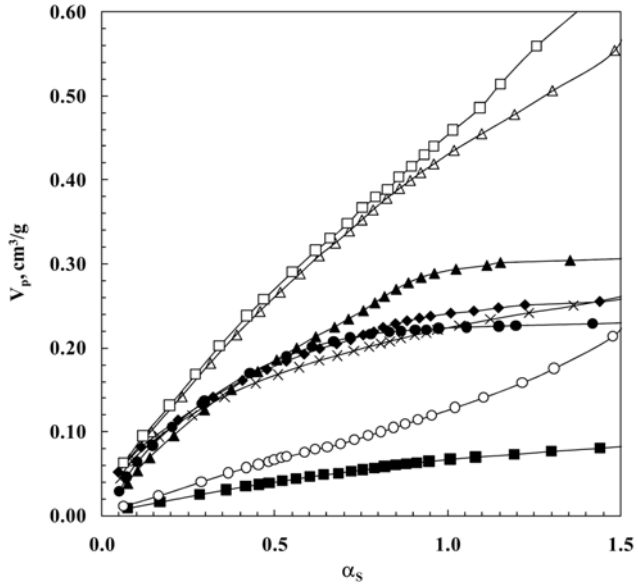

Fig. 4. α_s-plots for samples synthesized from $Na_2Si_3O_7$ and TEOS.
1-N: ●; 2-N: ▲; 3-N: ■; 4-VCO_2: ◆; 5-SCO_2: ×; 6-N: ○; 7-SCO_2: △; 8- SCO_2: □.

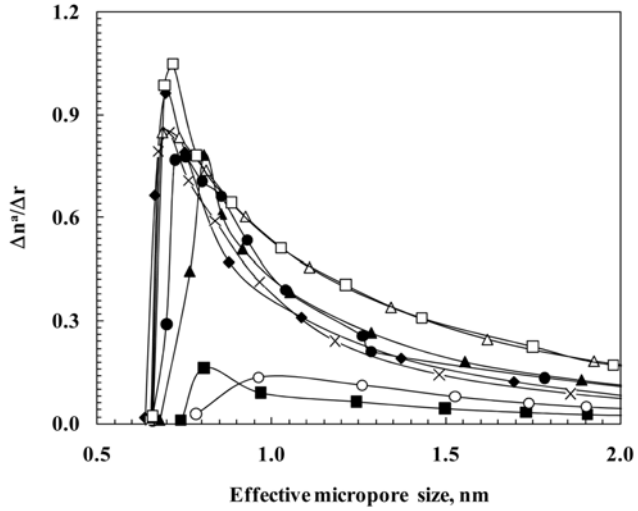

Fig. 5. Micropore size distribution for samples synthesized from $Na_2Si_3O_7$ and TEOS.
1-N: ●; 2-N: ▲; 3-N: ■; 4-VCO_2: ◆; 5-SCO_2: ×; 6-N: ○; 7-SCO_2: △; 8- SCO_2: □.

loops were attributed to the presence of predominantly micropores with very small amount of narrow slit-like mesopores. However, mesoporous silicas also exhibited similar hysteresis loops for cylindrical mesopores [31]. Interpreting very narrow hysteresis loops (almost within CSUs of experimental data points) between the adsorption and desorption branches of these nitrogen isotherms as the beginning of mesopore formation, we conclude, that 1-N and 2-N samples are predominantly microporous. Accordingly, the 3-N sample contains very small amounts of micro- and mesopores. From the shallow slope of these isotherms we conclude that these materials have small external area where multilayer nitrogen adsorption occurs [21]. The α_s-plot analysis revealed primary and secondary

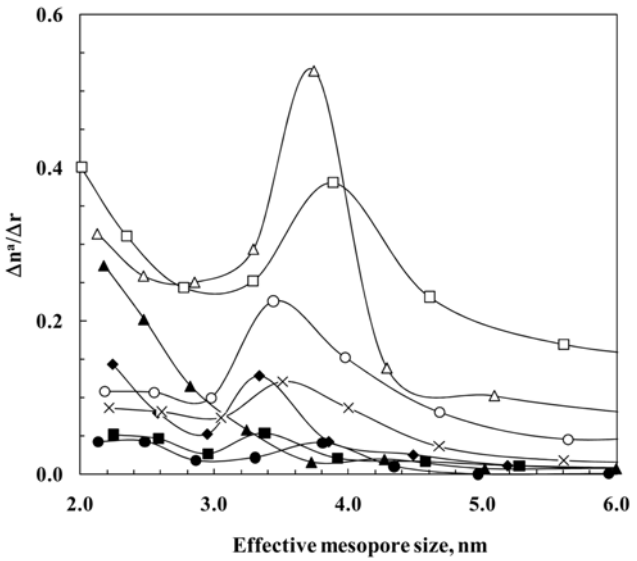

Fig. 6. Mesopore size distribution for samples synthesized from $Na_2Si_3O_7$ and TEOS.
1-N: ●; 2-N: ▲; 3-N: ■; 4-VCO_2: ◆; 5-SCO_2: ×; 6-N: ○; 7-SCO_2: △; 8- SCO_2: □.

micropore filling by nitrogen molecules. These micropores exhibit wide pore size distributions, which are visible from the shape of nitrogen adsorption isotherms with a gradual approach to full micropore filling occurring at 040-0.42p^o and pore size distribution curves shown in Fig. 5. Ryoo et al. [32] using $(w_{meso} \times A_{BET})/V_{pore}^{total}$-ratio explained the presence of microporosity in synthesized mesoporous silicas. In our case, this ratio varies from 4.2 to 8.4 for samples synthesized from $Na_2Si_3O_7$, and from 1.7 to 4.8 for samples synthesized from TEOS, with the higher values indicating the presence of greater degree of complementary intrawall micropores.

Different nitrogen adsorption behavior was observed for samples synthesized from TEOS (Fig. 3): all nitrogen isotherms are with limiting adsorption at high relative pressures of Type IV with H1 loop [30] or Type IVa [21]. The closure of desorption branches of nitrogen isotherms at relative pressures of 0.40-0.42p^o corresponding to the lower hysteresis limit for nitrogen adsorption at 77 K indicates capillary condensation with liquid-like nitrogen-adsorbate in mesopores [21]. Nitrogen isotherm for sample 8-SCO_2 is almost leveled off at pressures 0.9 to 1.0p^o. Extrapolation of linear α_s-plot resulted in negligible micropore volume; these silicas are predominantly mesoporous. Data from desorption branches of nitrogen isotherms were used for the evaluation of mesopore size distribution. As the result of sample calcinations, desorption branches of these nitrogen isotherms are non-vertical indicating to a broader mesopore size distribution (Fig. 5).

3. Effect of an Ageing Time

Ageing times of 6 and 24 hours were applied to samples 1-N and 2-N synthesized from $Na_2Si_3O_7$ at sub-critical conditions (room temperature and atmospheric pressure). The increase in the ageing time at 293.15 K caused an enhanced nitrogen adsorption by ≈34.0% at 0.95p^o and an increased A_{BET} by ≈10.4% (54.4 m^2/g) and V_{micro} by ≈26.9% (0.057 cm^3/g) due to a formation of new micropores with slightly wider effective diameter (0.81 nm). Mesopore volume constituted ≈9.8% of the total pore volume for sample 1-N, and for sample 2-N≈14.6% of the total pore volume. However, in absolute numbers mesopore volume has doubled (see Table 5) due to mesopore widening from 3.81 to 4.27 nm. A similar behavior was reported by Gobin et al. [33] for SBA-16 synthesized using TEOS.

4. Effect of Temperature and CO_2 Conditions

Physical properties such as diffusion coefficient, viscosity, and interfacial tension affect the overall supercritical and near-critical solution structure [11]. Although every effort was made to ensure uniform and equivalent mixing for both syntheses, clearly the silica source imparts considerably different particle growth dynamics, leading to a localized order and porosity. These differences in pore structure may be due to the differences in nucleation or transport processes [13,34]. At low-to-moderate pressures, Chun and Wilkinson [35] observed the reduction in interfacial tension of aqueous ethanol-CO_2 solutions with pressure. These authors indicate that this happens due to an increased solubility of CO_2 and its preference for the interface in the aqueous phase, which then translates to increased surface excess energy of the above solutions.

According to Table 2, a temperature increase from 293.15 to 338.15 K for 1-N and 3-N samples synthesized from $Na_2Si_3O_7$ dramatically reduced A_{BET} by ≈75.2% (379.0 m^2/g), V_{micro} by ≈68.4% (0.145 cm^3/g), but V_{meso} increased by ≈47.8% (0.011 cm^3/g), but still remained relatively low. Although the average micropore effective diameter increased slightly from 0.75 to 0.81 nm, the amount of micropores was significantly reduced. This was caused by intrawall micropores structure collapse to form smaller mesopores [36]. Consequently, mesopore volume increase was accompanied with a slight shift of average mesopore width from 3.9 to 3.4 nm. This is interpreted from the slight increase of hysteresis loop height (see Fig. 2).

Synthesis of 5-SCO_2 sample ($Na_2Si_3O_7$) compared to the sample 2-N reduced A_{BET} by ≈19.4% (108.2 m^2/g), reduced V_{micro} by ≈44.3% (0.119 cm^3/g), but appreciably increased Vmeso by ≈3.8 times (0.129 cm^3/g), suggesting that the formation of smaller mesopores (3.51 nm) occurred at the expense of intrawall micropores.

Although paying much attention to better solvating properties of LCO_2 and SCO_2, we observed that CO_2 in vaporous state with density of 158.47 kg/m^3 [28] also is able to develop mesopores (e.g., 4-VCO_2 in Tables 1 and 5). The slopes of the nitrogen isotherm increased together with the total nitrogen amount adsorbed as well as the hysteresis loop height when compared with sample 1-N. V_{micro} remained unchanged within CSUs, but v_{meso} increased almost three times, but still not significant in absolute value, ≈0.074 cm^3/g, while the mean mesopore width slightly reduced from 3.81 to 3.34 nm. Therefore, compared with the normal synthesis conditions, VCO_2 promotes mesopore formation.

A gradual increase in A_{BET} and mesopore volume was observed for samples synthesized from TEOS at supercritical CO_2 conditions (Table 5). An increase in V_{meso} of ≈77.1% (0.313 cm^3/g) was accompanied with increase in V_{micro} by ≈9.2 times (0.156 cm^3/g) for 7-SCO_2 sample. A further increase of V_{meso} up to 1.241 cm^3/g was observed for sample 8-SCO_2 synthesized at slightly different supercritical conditions. In this case, by lowering the temperature and pressure of CO_2 we increased its density from 483.58 to 566.31 kg/m^3 [28], thus improving the mesopore development. Synthesis conditions approaching critical promote mesopore formation, suggesting that the application of SCO_2 with its enhanced solvating properties is an appropriate technique for the formation of mesopores.

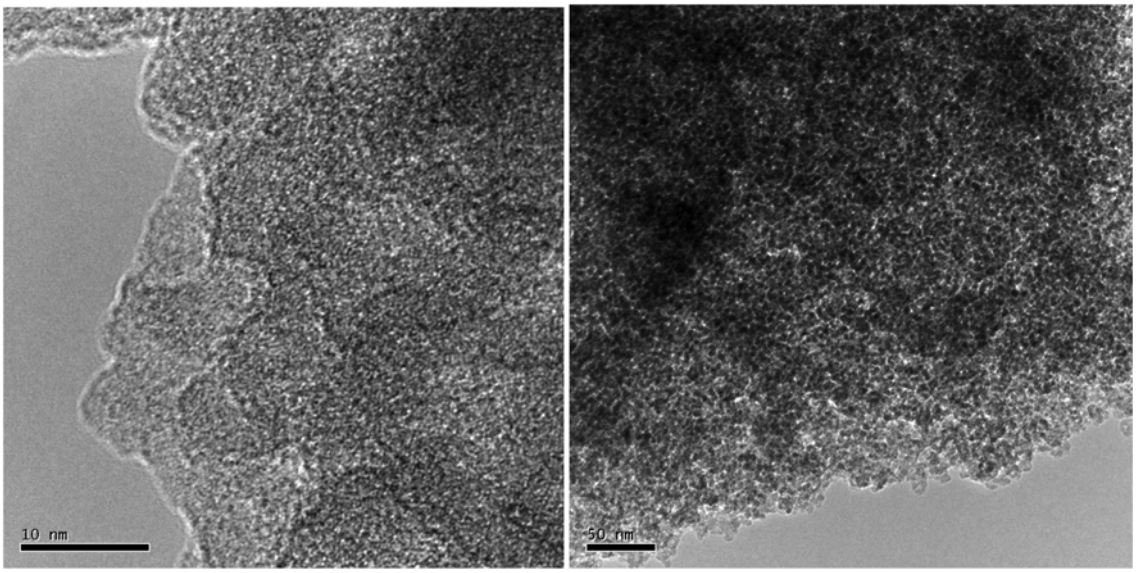

Fig. 7. TEM images of mesoporous silica sample 8-SCO_2.

According to Wakayama et al. [14], SCO_2 acts as an excellent solvent able to penetrate into the nano-scaled porous structures. Lower surface tension of SCO_2 also determines the amount of the solvent penetrating the matrix.

Disordered mesoporous structure of silicas synthesized from TEOS using SCO_2 in the present study is visible from the transmission electron micrograph (TEM) image for sample 8-SCO_2 (see Fig. 7). We obtained mesoporous silica with disordered wormhole-like pore structures. Similar mesoporous structures with pores sizes from 3.2 to 5.1 nm and A_{BET} varied from 525 to 1190 synthesized from TEOS using nonionic PEO surfactant as a neutral organic template were reported elsewhere [37,38]. Our SCO_2 synthesis conditions produced silicas with a higher mesopore volume - 1.241 against 0.90 cm^3/g [38].

5. Effect of Silica Source

Average micropore size for samples synthesized during the 'normal' procedure from $Na_2Si_3O_7$ and TEOS, 3-N and 6-N, respectively, is 0.81 and 0.96 nm (see Fig. 5). Synthesis by VCO_2 and SCO_2 led to a classical micropore formation for samples 4-VCO_2 and 7-SCO_2. All samples synthesized from TEOS exhibit higher mesopore width and greater mesopore volumes than those from $Na_2Si_3O_7$ as follows from Table 5 and Fig. 6. SCO_2 synthesis conditions have a more pronounced effect on the mesopore width for samples synthesized from TEOS.

CONCLUSIONS

The use of SCO_2 with TEOS leads to increased A_{BET}, micro- and mesopore volumes, compared with synthesis in aqueous and subcritical conditions. Sodium silicate has a lesser influence under similar conditions. Mesopore size distribution covers the range of pore width from about 3.51 to 3.88 nm for both silica source materials. Materials synthesized from sodium silicate and TEOS experienced enhanced adsorption, resulting in the increased amount of nitrogen adsorbed at $0.95P^0$. LCO_2 due to its higher solubility in polymeric template at below critical temperature better removes this template than SCO_2.

ACKNOWLEDGMENT

This research was supported by a 2003 Australia-Asia (Korea) Fellowship using facilities at the Center for Molecular and Materials Sciences, University of South Australia, and a grant (P-2004-09) from the Marine Bioprocess Research Center of the Marine Bio 21 Center funded by the Ministry of Maritime Affairs & Fisheries, Republic of Korea.

REFERENCES

1. A. E. C. Palmqvist, *Curr. Opin. Colloid Interface Sci.*, **8**, 145 (2003).
2. D. Zhao, J. Feng, B. F. Chmelk and G. D. Stucky, *J. American Chem. Soc.*, **120**, 6024 (1998).
3. J. P. Hanrahan, M. P. Copley, R. Spalding Trevor, J. D. Holmes, D. C. Steytler, H. Amenitsch, M. Steinhart and M. A. Morris, *J. Non-Cryst. Solids*, **353**, 4823 (2007).
4. R. F. Fulvio, S. Pikus and M. Jaroniec, *JMCh*, **15**, 5049 (2005).
5. R. V. Grieken, G. Calleja, G. D. Stucky, J. A. Melero, R. A. Garcia and J. Iglesias, *Langmuir*, **19**, 3966 (2003).
6. Q. S. Huo, J. L. Feng, F. Schuth and G. D. Stucky, *Chemistry of Materials*, **9**, 14 (1997).
7. C.-L. Lin, Y.-S. Pang, M.-C. Chao, B.-C. Chen, H.-P. Lin, C.-Y. Tang and C.-Y. Lin, *JPCS*, **69**, 415 (2008).
8. M.-C. Chao, C.-H. Chang, H.-P. Lin, C.-Y. Tang and C.-Y. Lin, *J. Mater. Sci*., **44**(24), 6453 (2009).
9. Y. Wan and D. Zhao, *Chem. Rev.*, **107**, 2821 (2007).
10. T.-W. Kim, R. Ryoo, M. Kruk, K. P. Gierszal, M. Jaroniec, S. Kamiya and O. Terasaki, *J. Phys. Chem. B*, **108**, 11480 (2004).
11. A. I. Cooper, *Advanced Materials*, **13**, 1111 (2001).
12. J. P. Hanrahan, M. P. Copley, K. M. Ryan, T. R. Spalding, M. A. Morris and J. D. Holmes, *Chem. Mater.*, **16**, 424 (2004).
13. M. A. McHugh and V. J. Krukonis, *Supercritical fluid extraction (principles and practice); chemical reaction in supercritical fluids*,

2nd edition, Butterworth-Heinemann, Boston (1994).
14. H. Wakayama, Y. Goto and Y. Fukushima, *Physical Chemistry Chemical Physics*, **5**, 3784 (2003).
15. T. Tsoncheva, J. Rosenholm, M. Linden, L. Ivanova and C. Minchev, *Appl. Catal. A: Gen.*, **318**, 234 (2007).
16. S. Kawi and M. W. Lai, *AIChE J.*, **48**, 1572 (2002).
17. A. Badalyan, P. Pendleton and H. Wu, *Rev. Sci. Instrum.*, **72**, 3038 (2001).
18. A. Badalyan and P. Pendleton, *Langmuir*, **19**, 7919 (2003).
19. S. J. Gregg and K. S. W. Sing, *Adsorption, surface area and porosity*, Academic Press, London (1982).
20. A. Badalyan and P. Pendleton, *J. Colloid Interface Sci.*, **326**, 1 (2008).
21. F. Rouquerol, J. Rouquerol and K. S. W. Sing, *Adsorption by powders and porous solids*, Academic Press, Sydney (1999).
22. IUPAC, *Pure Appl. Chem.*, **66**, 1739 (1994).
23. A. Saito and H. C. Foley, *AIChE J.*, **37**, 429 (1991).
24. A. C. Lasaga and R. T. Cygan, *AmMin*, **67**, 328 (1982).
25. H.-Y. Kim, J. O. Sofo, D. Velegol, Cole, Milton W. and G. Mukhopadhyay, *PhRvA*, **72**, 053201 (2005).
26. *CRC handbook of chemistry and physics*, 85th Edition, CRC Press (2004).
27. E. P. Barrett, L. G. Joyner and P. P. Halenda, *J. American Chem. Soc.*, **73**, 373 (1951).
28. R. Span and W. Wagner, *JPCRD*, **25**, 1509 (1996).
29. Y. Sato, T. Takikawa, M. Yamane, S. Takishima and H. Masuoka, *Fluid Phase Equilib.*, **194-197**, 847 (2002).
30. IUPAC, *Pure Appl. Chem.*, **57**, 603 (1985).
31. P. J. Kooyman, M. J. Verhoef and E. Prouzet, *Stud. Surf. Sci. Catal.*, 129 (Nanoporous Materials II, Proceedings of the Conference on Access in Nanoporous Materials, 2000), 535 (2000).
32. R. Ryoo, C. H. Ko, M. Kruk, V. Antochshuk and M. Jaroniec, *J. Phys. Chem. B.*, **104**, 11465 (2000).
33. O. C. Gobin, Y. Wan, D. Zhao, F. Kleitz and S. Kaliaguine, *J. Phys. Chem. C*, **111**, 3053 (2007).
34. Y. Arai, T. Sako and Y. Takebayashi, *Supercritical fluids: Transport properties of supercritical fluids*, Springer-Verlag, New York (2001).
35. B. S. Chun and G. T. Wilkinson, *Ind. Eng. Chem. Res.*, **34**, 4371 (1995).
36. A. Galarneau, H. Cambon, F. Di Renzo, R. Ryoo, M. Choi and F. Fajula, *New Journal of Chemistry*, **27**, 73 (2003).
37. S. A. Bagshaw, E. Prouzet and T. J. Pinnavaia, *Science*, **269**, 1243 (1995).
38. S.-S. Kim, T. R. Pauly and T. J. Pinnavaia, *ChCom*, **10**, 835 (2000).